Chemical Disorder Reinforces Magnetic Order in Ludwigite $(Ni,Mn)_3BO_5$ with Mn^{4+} Inclusion

Svetlana Sofronova [a], Evgeniya Moshkina [a,b], Ilya Nazarenko [a], Alexey Veligzhanin [c], Maxim Molokeev [d], Evgeniy Eremin [a,d], Leonard Bezmaternykh [a]

[a] *L.V. Kirensky Institute of Physics SB RAS, 660036 Krasnoyarsk, Russia*
[b] *Siberian State Aerospace University named after Academician M.F. Reshetnev, 660037 Krasnoyarsk, Russia*
[c] *National Research Centre "Kurchatov Institute", 123182 Moscow, Russia*
[d] *Siberian Federal University, 660041 Krasnoyarsk, Russia*

Abstract

Crystals of ludwigite $Ni_{2.14}Mn_{0.86}BO_5$ were synthesized by flux growth technique and contain Mn^{3+} and Mn^{4+}. A possible mechanism of the manganese valence states stabilization has been proposed. The structural and magnetic characterization of the synthesized samples has been carried out in detail. The cations composition and Mn valence states of the crystal were determined using X-ray diffraction and EXAFS technique. The comparative analysis was carried out between the studied crystal and Ni_2MnBO_5 synthesized previously. Magnetic susceptibility measurements were carried out. The magnetic transition in the studied composition occurs at the 100 K temperature that is higher than in Ni_2MnBO_5 although the studied composition is more disordered. The calculations of the exchange integrals in the frameworks of indirect coupling model revealed strong antiferromagnetic interactions. The several magnetic subsystems existence hypothesis was supposed. The possible magnetic structure was suggested from the energies estimation for different ordering variants.

Keywords

oxide, oxyborate, magnetism, crystal growth, EXAFS

Introduction

Oxiborates Ni_{3-x} Mn_xBO_5 belong to the family of ludwigites [1]. The peculiarity of these compounds is the presence of quasi-low-dimensional elements in the structure - three-legged ladders, as well as triangular groups, which in some cases leads to very interesting physical properties. In addition to this, there are different valence metal ions in the structure, they can be di- and tri- [2, 3], as well as di- and tetravalent ions [4, 5, 6].

There are monometallic ludwigites: Fe_3BO_5 and Co_3BO_5, in which Fe (Co) ions are represented in the di- and trivalent state. Both compounds exhibit interesting physical properties.

In Fe_3BO_5 at high temperatures, ions with spins 5/2 are localized in one of the subsystems formed by Fe^{3+}-Fe^{2+}-Fe^{3+} ions, and one additional electron is smeared out between three ions. With increasing temperature, this additional electron is localized in one of the pairs, as a result, a dimer is formed, and a structural phase transition occurs with an increase in the crystalline cell by the factor of two. In addition, a singularity is also observed on the magnetization curves. Magnetic ordering occurs at lower temperatures in two stages: at 112 K and 74 K, while the two subsystems are ordered mutually orthogonally. [3]

In Co_3BO_5, charge ordering arises immediately at high temperatures, and unlike iron ludwigite, magnetic ordering occurs in one stage at 42 K. However, the Co^{3+} ion is in the low-spin state, and its spin is zero. Apparently, the transition to the low-spin state of the Co^{3+} ion and the mutual orthogonal orientation of the two magnetic subsystems in Fe_3BO_5 arises to reduce frustrations in the system [3, 7].

It is interesting to prepare other compounds in which a magnetic ion would be present in different valence states. The manganese ion is found in compounds in di-, tri-, and tetravalent states.

It is known that there is a Ni_2MnBO_5 compound, where the manganese ion is in the tetravalent state. We have obtained and investigated the compound Ni_2MnBO_5, where the manganese ion is in the trivalent state [8]. In this paper, we present an attempt to obtain the ludwigite $Ni_{3-x}Mn_xBO_5$, in which the manganese ion would be represented in the tri- and tetravalent state. We also investigate the effect of a tetravalent manganese ion presence on physical properties.

1. Synthesis

The physical properties of ludwigites are very sensitive to the changes in the composition, even within the small limits. Therefore, in the synthesis of such compounds, a special role is played by controlling the valence state of the metallic cations. The synthesis of ludwigites with a certain composition involves the development of a growing technique that will allow us to determine the factors that affect the conversion of the transition metals cations valence states, especially Mn cations.

Initially, the hypothesis of the Mn-heterovalent (containing Mn^{3+}, Mn^{4+}, and maybe Mn^{2+}) ludwigite $Ni_{3-x}Mn_xBO_5$ existence was made on the basis of the criterion presented in [9], which consists in a certain ratio of the radius of the tetra- / trivalent cation to the divalent radius.

1.1. Flux Growth Technique

$Mn_{0.86}Ni_{2.14}BO_5$ single crystals were synthesized from the flux with an initial molar ratio of the components $Bi_2Mo_3O_{12}$:1.6B_2O_3:0.84Na_2O:0.94NiO:0.178Mn_2O_3.

The flux in a mass of 67 g was prepared from initial oxides Mn_2O_3 and NiO in combination with sodium carbonate at the temperature T = 1100°C in a platinum crucible with the volume V = 100 cm^3 by sequential melting of powder mixtures, first $Bi_2Mo_3O_{12}$, and B_2O_3, then Mn_2O_3 and NiO; finally, Na_2CO_3 was added in portions.

In the prepared flux, the phase crystallizing within a sufficiently wide (about 40°C) high-temperature range was $Mn_{3-x}Ni_xBO_5$ with the ludwigite structure. The saturation temperature of the flux was T_{sat} = 920°C.

Single crystals of the ludwigites were synthesized by spontaneous nucleation. After homogenization of the flux at T = 1100°C for 3 h, the temperature was first rapidly reduced to (T_{sat}–10)°C and then slowly reduced with a rate of 4°C/day. In 3 days, the growth was completed, the crucible was withdrawn from the furnace, and the flux was poured out. The grown single crystals in the form of orthogonal prisms with a length of 6 mm and a transverse size of about 0.3 mm were etched in a 20% water solution of nitric acid to remove the flux remainder.

1.2. Manganese Valence State Conversion Mechanism

The synthesis of the single crystals containing the multiple-valence cations of the same element is a complex problem since the relative content of such cations cannot be often controlled due to valence conversion at the high temperatures. In the synthesis of heterovalent oxyborates with a ludwigite structure, the mechanism for stabilizing valence states of transition metal cations is not clearly defined for many systems in particular, and moreover, there is no universal technique.

Depending on the type of cation, several methods of heterovalent oxyborates single crystal synthesis are known. In the framework of these methods, the stabilization of valence states was carried out by maintaining the atmosphere of argon [10] or oxygen [11], with the help of the Fe metal chips additives

when growing ludwigite Fe_3BO_5 [12, 13], under high-pressure conditions [12]. Many methods for growing such single crystals involve the use of the borax $Na_2B_4O_7$ [14, 15] or boric acid H_3BO_3 [16, 15], the effect of these components on the stabilization of valence states of transition metal cations has not been reported. In a number of cases, the combined crystallization of ludwigites and oxides (Fe_3O_4, Fe_2O_3, Mn_2O_3, Co_2O_3) was observed [10, 17, 2].

As was shown in the previous section, the operating temperature of alloying the initial components of the solution-melt is 1100°C. This temperature is higher than the decomposition temperature of the oxide $6Mn_2O_3 \xrightarrow{1080°C} 4Mn_3O_4 + O_2$, as a result of which the valence of manganese partially changes and an uncertainty arises over the composition of the flux. In the synthesis of Mn-heterovalent ludwigite $Ni_{3-x}Mn_xBO_5$ at $x > 2$ (with the presence of the Mn^{4+} cation) with the help of the flux method, it is assumed in this paper that the components of the $Bi_2Mo_3O_{12}$ and Na_2CO_3 solvent play a special role in the stabilization of manganese in the divalent and trivalent state, respectively, at the temperature of the flux preparing.

When the initial components are fused, it is assumed that the hierarchy of chemical bonds is such that due to the interaction between Mn_2O_3 manganese trioxide and MoO_3 molybdenum trioxide, which is released from $Bi_2Mo_3O_{12}$, the following reaction occurs with the formation of $Mn^{2+}MoO_4$ intermediate bonds, which keep manganese in a state with valence 2+:

$$4Bi_2Mo_3O_{12} + 6Mn_2O_3 \rightarrow 12MnMoO_4 + 4Bi_2O_3 + 3O_2 \uparrow$$

It is also assumed that due to the interaction of manganese trioxide Mn_2O_3 and sodium carbonate Na_2CO_3, the following reaction occurs:

$$Mn_2O_3 + Na_2CO_3 \rightarrow 2NaMn^{3+}O_2 + O_2 + CO_2 \uparrow$$

As a result of this reaction, intermediate bonds of the Delafossite type $NaMn^{3+}O_2$ are formed in the solution-melt, which makes it possible to retain manganese in a trivalent state.

Thus, in NiO and Mn_2O_3 solutions in Bi_2O_3-B_2O_3 melts diluted with Na_2CO_3 and MoO_3, it is possible to stabilize Mn^{2+} by a $Mn^{2+}MoO_4$ bond and Mn^{3+} by a bond of $NaMn^{3+}O_2$ types. As shown by our experiments, the connection of the second type prevails. Therefore, in molten solutions with a large ratio of NiO to $NaMn^{3+}O_2$, the crystallization of the ludwigite phase $Ni^{2+}_{2+x}Mn^{3+}_{1-2x}Mn^{4+}_{x}BO_5$ ($0 \le x \le 0.5$) is determined by two processes:

(I) $$2NiO + NaMnO_2 + \frac{1}{2}B_2O_3 \rightarrow Ni_2Mn^{3+}BO_5 + \frac{1}{2}Na_2O$$

(II) $$2.5NiO + NaMnO_2 + \frac{1}{2}B_2O_3 \rightarrow Ni_{2.5}Mn^{4+}_{0.5}BO_5 + \frac{1}{2}Na_2O + \frac{1}{2}MnO$$

It is the second process that is responsible for the conversion of $Mn^{3+} \rightarrow Mn^{4+}$.

Using this technique, a number of compounds with different contents of nickel and manganese was obtained.

2. Crystal Structure

The powder diffraction data of the studied sample for Rietveld analysis was collected at room temperature with a Bruker D8 ADVANCE powder diffractometer (Cu-Kα radiation) and linear VANTEC detector. The step size of 2θ was 0.016°, and the counting time was 3 s per step. The 2θ range of 5-70° was measured with 0.6 mm divergence slit, but the 2θ range of 70-140° was measured with 2 mm divergence slit. Larger slits allow noticeably increase the intensity of high-angle peaks without loss of resolution because the high-angle peaks are broad enough to be not affected by bigger divergence beam. The esd's $\sigma(I_i)$ of all points on patterns were calculated using intensities I_i: $\sigma(I_i)=I_i^{1/2}$. The intensities and obtained esd's were further normalized: $I_{i\,\mathrm{norm}} = I_i \times 0.6/(\text{slit width})$, $\sigma_{\mathrm{norm}}(I_i) = \sigma(I_i) \times 0.6/(\text{slit width})$, taking into account actual value of divergence slit width which was used to measure each

particular intensity I_i and saved in an xye-type file. So transformed powder pattern has usual view in whole 2θ range 5-140°, but all high-angle points have small esd's.

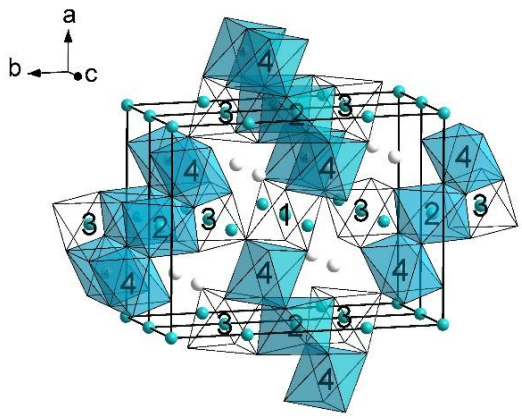

Figure 1. The structure of the studied crystal. The site 4 is occupied randomly by Mn and Ni ions. Crystallographic positions are 1 – 2a, 2 – 2d, 3 – 4g, 4 – 4h.

Rietveld refinement was performed by using TOPAS 4.2 [9] which accounts esd's of each point by special weight scheme. All peaks were indexed by orthorhombic cell (*Pbam*). The unit cell contains two formula units (Figure 1). Metallic ions occupy four positions, in Figure 1, they are indicated by the numbers 1-4. In most ludwigites, positions 1-3 are often occupied by divalent cations, while the position 4 is occupied by trivalent cations (either tetravalent and divalent in the ratio 1:1). The crystal structure of $Mn_{0.5}Ni_{2.5}BO_5$ [10] was taken as starting model for Rietveld refinement. Within the framework of this method, it is difficult to clarify the composition and population of atoms by positions, so we believed that all Mn/Ni sited was 0.25/0.75 according to the chemical formula of $Mn_{0.5}Ni_{2.5}BO_5$ by Mn and Ni ions with fixed occupations. In order to reduce the number of refined parameters, only one thermal parameter was refined for all O atoms. Refinement was stable and gives low R-factors (Table 1, Figure 1). Coordinates of atoms and main bond lengths are in Table 2. For comparison in Table 1, the lattice parameters for the Ni_2MnBO_5 [11] compound are also given, which we will need later in our discussion.

Table 1. Main parameters of processing and refinement of the studied sample.

Compound	**Studied sample**	**Ni_2MnBO_5** [12]
Sp.Gr.	Pbam	Pbam
a, Å	9.1650 (2)	9.176(1)
b, Å	12.2545 (3)	12.316(2)
c, Å	2.98895 (5)	2.9978(4)
V, Å^3	335.69 (1)	338.78(8)
Z	4	4
2θ-interval, °	5-140	
R_{wp}, %	1.92	
R_p, %	1.57	
R_{exp}, %	1.28	
χ^2	1.50	
R_B, %	1.53	

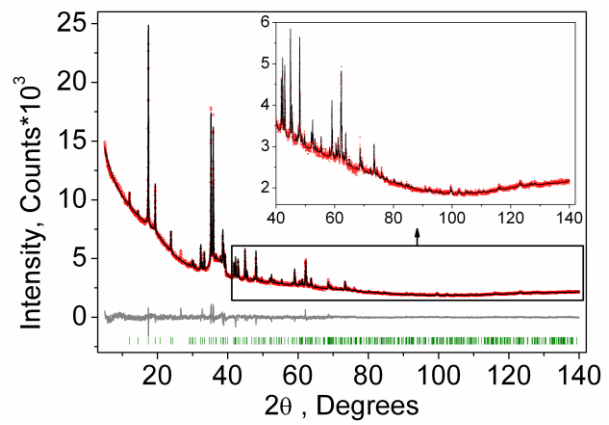

Figure 2. Difference Rietveld plot of the studied sample.

Table 2. Fractional atomic coordinates and isotropic displacement parameters (Å^2) of the studied sample.

	x	*y*	*z*	B_{iso}	Occ.
Mn1	0	1	0	3.2 (4)	0.25
Mn2	0	0.5	-0.5	3.0 (4)	0.25
Mn3	-0.002 (1)	0.7220 (3)	0	2.7 (4)	0.25
Mn4	0.2584 (7)	0.6180 (5)	-0.5	2.1 (4)	0.25
Ni1	0	1	0	3.2 (4)	0.75
Ni2	0	0.5	-0.5	3.0 (4)	0.75
Ni3	-0.002 (1)	0.7220 (3)	0	2.7 (4)	0.75
Ni4	0.2584 (7)	0.6180 (5)	-0.5	2.1 (4)	0.75
B	0.222 (5)	0.868 (4)	-0.5	3 (1)	1
O1	-0.107 (2)	0.860 (1)	0	2.6 (4)	1
O2	0.155 (2)	0.765 (2)	-0.5	2.6 (4)	1
O3	0.102 (2)	0.577 (1)	0	2.6 (4)	1
O4	-0.150 (2)	0.647 (2)	-0.5	2.6 (4)	1
O5	0.147 (2)	0.948 (1)	-0.5	2.6 (4)	1

2.1. EXAFS

The composition of the studied compound was refined by studying the XAS at the K-edge of manganese and nickel ions. X-ray absorption spectra were measured at the experimental station "Structural Material Science" of the Kurchatov synchrotron radiation source [13]. The experimental procedure and technique of processing and analyzing the results have been described in detail in the paper [14].

To compensate the decrease in the amplitude of the EXAFS oscillations with increasing energy, the exposure time *T* at the points after the absorption edge was increased according to the quadratic law ($T = a \cdot n^2 + c$), depending on the number of the point *n*. The adjustment constants *a* and *c* of this expression were chosen so that the initial exposure of 1 second at the end of the measurement area was 4 seconds. Thus, each spectrum was measured for approximately 20 minutes. To improve the statistics, each sample was measured for 2-3 times, after which the spectrum was averaged.

The processing and analysis of the results were carried out using the IFEFFIT [15, 16] program version 1.2.11c. The measured XAFS data were first processed by the ATHENA program of this complex to adjust the background, normalize the spectra to a unity-height jump, and obtain the oscillating part of the spectrum. The fine structure of the X-ray absorption spectrum obtained in this manner after the *K*-jump was then used for the structural analysis.

The parameters of the local structure around the absorbing atom were determined by fitting the model spectrum to the experimental spectrum of EXAFS. The number of coordination spheres was adjusted for each of the absorbing atoms separately and in the final model, two coordination spheres for the nickel atom and five coordination spheres for the manganese atom were used. Such a simulation made it possible to refine the distances from the absorbing atom to the nearest neighbors R_j, a *mean-square variation of the bond length* σ_j^2 for atomic pairs, taking into account thermal vibrations and static disordering of the local environment. The coordination numbers N_j of the nearest neighbors relative to the central metal atom were fixed in accordance with the structural model of the studied samples. The photoelectron energy shift value ΔE_0 relative to the position of the absorption *K*-edge and the damping coefficient of the signal amplitude S_0^2 were also included in the refinement (Table 3).

Table 3. Parameters of the nearest environment of Ni and Mn obtained by fitting EXAFS data.

Ion	R_f,%	*k*-range	*R*-range	S_0^2	E_0,eV	The scattering path	*N*	*R*, Å	σ^2, Å^{2}x10^{-3}
Mn	7.78	2.000 - 12.000	1.0 - 4.2	0.63±0.18	0.39±2.71	Mn-O1	4.0	1.91(3)	6±3
						Mn-O2	2.0	2.11(6)	
						Mn-Mn1(Ni)	1.0	2.81(5)	5±2
						Mn-Mn2(Ni)	6.0	3.05(1)	
						Mn-Mn3(Ni)	2.0	3.33(3)	
Ni	1.9	2.000 - 12.000	1.15 - 3.25	0.58±0.06	1.65±1.1	Ni-O	6.0	2.081(8)	4±1
						Ni-Mn(Ni)	8.0	3.072(8)	8±1
Ni	1.5	2.000 - 12.000	1.15 - 3.25	0.59±0.06	2.15±1.1	Ni-O	6.0	2.083(8)	4±1
						Ni-Mn1(Ni)	6.0	3.055(9)	5±1
						Ni-Mn2(Ni)	2.0	3.18(4)	5±1

The local environment of nickel is characterized by a relatively small value of the parameter S_0^2, which may be due to some distortion of the octahedral environment. However, attempts to describe this distortion by adding an additional nonequivalent Ni-O distance do not improve the fit.

The results of fitting the Fourier transform and the oscillating part of the EXAFS spectra are shown in Figure 3, Figure 4.

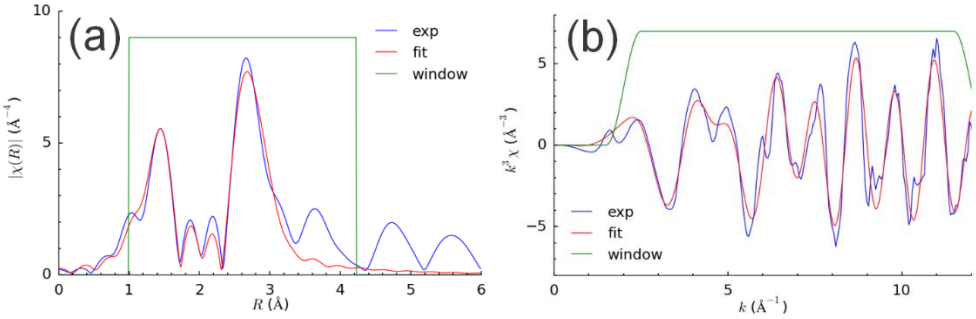

Figure 3. FT and an oscillating part of the manganese spectrum for the studied sample.

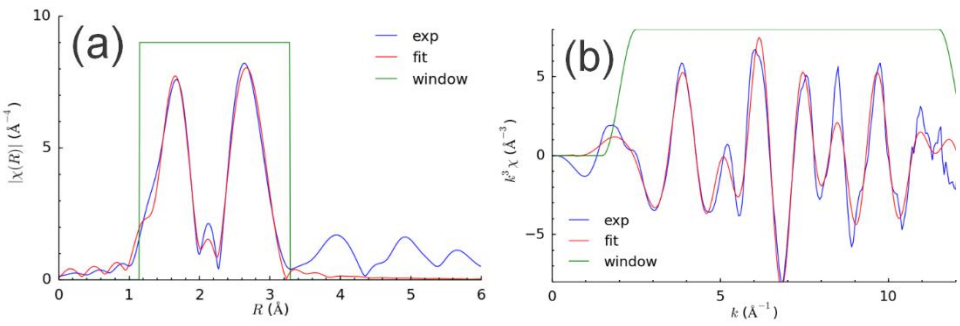

Figure 4. FT and the oscillating part of the nickel spectrum for the studied sample.

The composition of the compound was refined by the jump in the K-edge of the manganese and nickel absorption spectrum. As a result of the refinement, the following formula of the compound was obtained: $Ni_{2.14}Mn_{0.86}BO_5$. The obtained composition completely corresponds to the composition "by laying".

The valence of metal ions was studied by the fingerprint method. Comparison of the spectra of the K-edge of nickel with the NiO standard shows good agreement (Figure 5), in addition, it can be seen from the figure that the spectra of the composition of Ni_2MnBO_5 and the composition under study also coincide. We believe that the nickel in the ludwigites is present only in the divalent state.

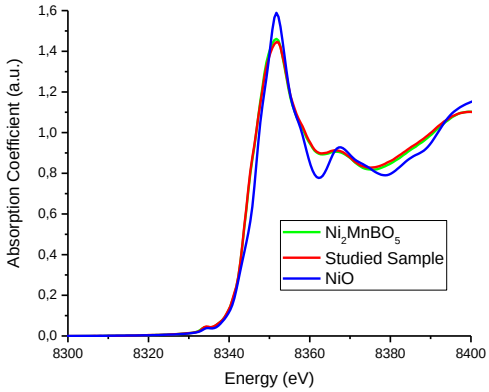

Figure 5. K-absorption edge of Ni for the studied sample.

For the manganese oxidation degree analysis, the XANES region of absorption specter and the first derivative of the specter were compared with corresponding spectra of well-characterized standards - MnB_2O_4 (Mn II), $Mn_{1-x}Fe_xMoO_4$ (Mn II), Mn_2O_4 (Mn III) и MnO_2 (Mn IV) (Figure 6).

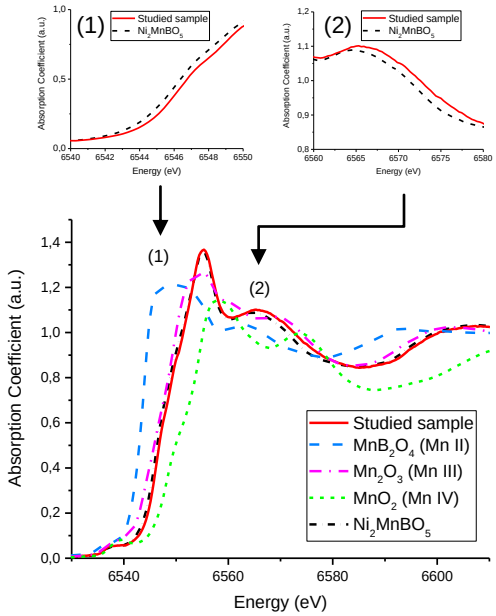

Figure 6. K-absorption edge of Mn and comparison insets of studied sample and Ni_2MnBO_5.

Mn K-edge absorption spectrum of the studied composition differs from the Ni_2MnBO_5 spectrum, where manganese is supposedly included only in the trivalent state. There is a shift of the spectrum to the higher energy, which corresponds to some increase in the Mn valence. To maintain electroneutrality, when the divalent ion (Ni) content in the composition is greater than 2, the presence of tetravalent ion

is necessary. The composition and the displacement of the absorption spectrum of manganese K-edge indicate the presence of manganese in two valence states: 3- and 4-valent.

Table 4 shows the parameters of the local structure of the Ni_2MnBO_5 crystal and the $Ni_{2.14}Mn_{0.86}BO_5$ around Mn atoms, determined with the same initial model. The presence of the ion with a smaller ionic radius manifests itself by the substantial Mn-O bond decrease. Ni-O bonds are also shortened, but to a lesser extent, that is likely related to a decrease in the lattice parameters (Table 4). The Mn-O octahedron is quite distorted and means a local structure, it can be described by two long and four short bonds, Ni-O octahedra are apparently more balanced, and the difference of Ni-O bonds as it is observed by X-ray diffraction cannot be resolved by EXAFS.

Thus, we have confirmed that we obtained a composition in which manganese is included in different valence states: tri- and tetravalent.

Table 4. The bond lengths obtained in the compositions of the nickel-manganese ludwigites.

Composition	**Mn-O**		**Ni-O**	
	4 bonds	2 bonds	6 bonds	6 bonds
Ni_2MnBO_5	1.95	2.17	2.087	2.091
$Ni_{2.14}Mn_{0.86}BO_5$	1.91	2.11	2.081	2.083

3. Magnetic Properties

Magnetic measurements of $Ni_{2.14}Mn_{0.86}BO_5$ were performed using the physical properties measurements system PPMS-9 (Quantum Design) at temperature range T=3÷300 K and magnetic fields up to 80 kOe. The studies were carried out on small single crystals, each of which was randomly oriented to obtain isotropic magnetization. The temperature dependence of the magnetization in the fields of 1, 5 and 10 kOe is shown in Figure 7. As can be seen from the figure, in the region of 100 K, an ordering of the magnetic moments occurs, the magnetization increases and decreases below 30 K, which is typical for the disordered systems. Temperature dependence of the inverse magnetic susceptibility $1/\chi=B/M$ of ludwigite $Ni_{2.14}Mn_{0.86}BO_5$ is shown in Figure 7b (inset).

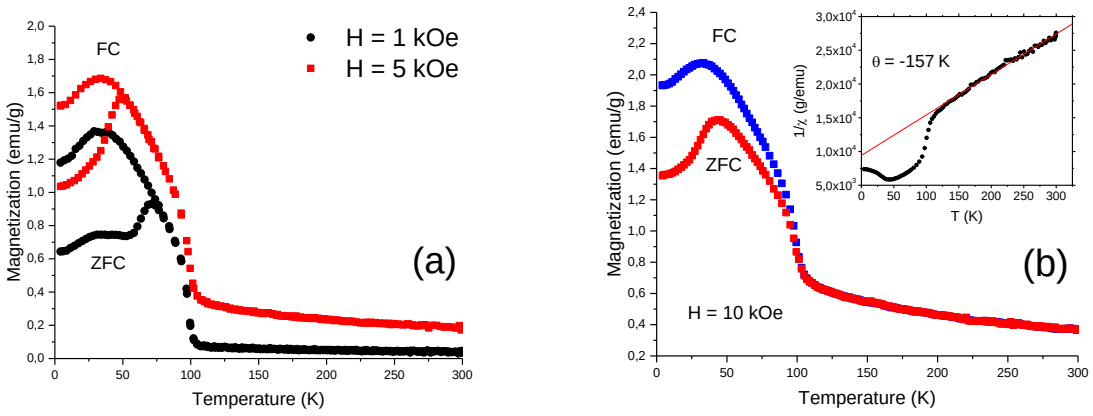

Figure 7. (a) - magnetization versus temperature for the studied composition in the fields 1 and 5 kOe; (b) - magnetization versus temperature for the studied composition in a field of 10 kOe, the inset shows the inverse susceptibility versus temperature for the studied compound.

It should be noted that the magnetic ordering temperature for the studied composition is 15 K higher than Ni_2MnBO_5 composition. However, as in Ni_2MnBO_5, there is a feature on the magnetization curves at the 60 K. [11]

The fitting of the temperature dependence of magnetic susceptibility of paramagnetic phase was performed using the modified Curie–Weiss law ($T = 200 \div 300\mathrm{K}$):

$$\chi = \chi_0 + \frac{C}{T - \theta}$$

The parameters of this dependence were determined. Temperature-independent term, which includes diamagnetic contribution of completely filled electron shells and Van Vleck paramagnetism, is a positive $\chi_0 \approx 0.22 \cdot 10^{-4}$ emu/mol (diamagnetic contribution to χ_0 was calculated by summing the diamagnetic Pascal constants of each ion and it is $\chi_D \approx -0.94 \cdot 10^{-4}$ emu/mol [17]. Negative sign of Weiss temperature $\theta = -157$ K indicates the strong antiferromagnetic interactions in the crystal. In addition, as a result of approximation, the value of Curie constant of studied ludwigite was obtained, and it is $C \approx 4.4$ emu · K/mol. Using this parameters, the effective magnetic moment of the formula unit was estimated via relation $\mu_{eff}^{exp\,2} = 8C$, and it is $\mu_{eff}^{exp} \approx 5.93\ \mu_B$/mol. Effective magnetic moment also was calculated theoretically via $\mu_{eff}^{theor} = \sum(Ng^2S(S+1)\mu_B^2)^{1/2}$ (only spin component of the effective magnetic moment was taken into account), where *N* is composition *x*, *g* is g-factor of ions Mn^{3+} (*g*=2 [18]), Mn^{4+} (*g*=1.96 [19]) and Ni^{2+} (*g*=2.08 [20]) in octahedral coordination, obtained in other works. Calculated value of effective magnetic moment $\mu_{eff}^{theor} \approx 6.19\ \mu_B$/mol agrees with the value of experimentally estimated effective magnetic moment $\mu_{eff}^{exp} \approx 5.93\ \mu_B$/mol within the error determination of Curie constant *C* and corresponds to the high-spin states *S*(Ni^{2+})=1, *S*(Mn^{3+})=2, *S*(Mn^{4+})=3/2.

Residual magnetization in the studied composition is 0.021 μ_B/mol, and in Ni_2MnBO_5 [11], it is 0.079, 0.069, 0.025 μ_B/mol at 3, 20, 50 K, respectively.

Below the magnetic transition temperature, unlike Ni_2MnBO_5, remanence does not vary, though it is smaller than Ni_2MnBO_5. Apparently, the Mn^{4+} appearance in the composition reduces exchanges competition in the system and helps to stabilize the magnetic structure at the higher temperature than in Ni_2MnBO_5.

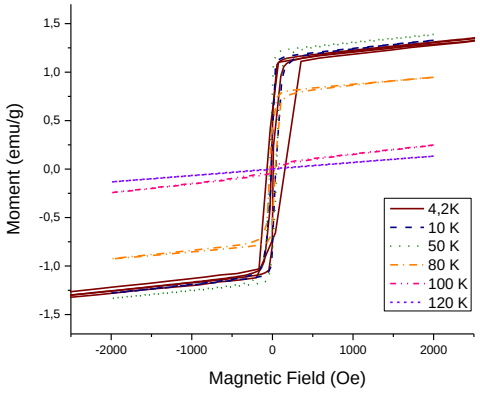

Figure 8. The studied sample field dependencies of the magnetization.

3.1. Calculation of the Exchange Interactions

We tried to analyze the exchange interactions in $Ni_{2.14}Mn_{0.86}BO_5$ in the framework of the Andersen-Zawadsky's indirect exchange model [21] to understand the possible reasons for increasing the magnetic ordering temperature. Model parameters were taken from [22]. The results of the calculation and comparison with Ni_2MnBO_5 are shown in Table 5.

We believe that the position 4 is occupied by 0.14 of Ni^{2+}, 0.14 of Mn^{4+} and 0.72 of Mn^{3+}, in the third column, there are average values of the indirect exchange interaction, and in the last column, there are values for each type of ions.

Table 5. Comparison of the exchange interaction values for both compositions of nickel-manganese ludwigites.

Pos.	Angles	Expression	Occ.	J(studied	J(Ni_2MnBO_5)

				sample)	
4-4	α = 93° β = 99°	$\frac{2c}{27}(4bJ_{Mn^{4+}} - 3cU_{Mn^{4+}})(\sin\alpha + \sin\beta) = -0{,}085\ K$	0.020	-2.437	-1.815
		$\frac{c}{3}\left(3cJ_{Ni^{2+}} - 4b(U_{Mn^{4+}} + U_{Ni^{2+}})\right)(\sin\alpha + \sin\beta) = -7{,}805\ K$	0.040		
		$\frac{2}{3}bcJ_{Ni^{2+}}(\sin\alpha + \sin\beta) = 5{,}527\ K$	0.020		
		$\frac{2c}{48}(3bJ_{Mn^{3+}} - (3c + 2b)U_{Mn^{3+}})(\sin\alpha + \sin\beta) = -1{,}826\ K$	0.518		
		$\frac{c}{36}\left(b(4J_{Mn^{3+}} + 3J_{Mn^{4+}}) - (3c + b)(U_{Mn^{4+}} + U_{Mn^{3+}})\right)(\sin\alpha + \sin\beta) = -1{,}314\ K$	0.202		
		$\frac{c}{24}\left((3c + b)J_{Mn^{3+}} - 4b(U_{Ni^{2+}} + U_{Mn^{3+}})\right)\sin\alpha = -5{,}156\ K$	0.202		
3-3	α = 90.4° β = 91°	$\frac{8}{3}bcJ_{Ni}(\sin\alpha + \sin\beta)$	1	5.570	5.570
2-2	α = β = 92°		1	5.564	5.564
1-1	α = β = 91°		1	5.568	5.568
4-2	α = 84°	$\frac{c}{9}\left(3cJ_{Ni^{2+}} - 4b(U_{Mn^{4+}} + U_{Ni^{2+}})\right)\sin\alpha = -7{,}828\ K$	0.140	-4.020	-5.139
		$\frac{2}{3}\ bcJ_{Ni^{2+}}\sin\alpha = 5{,}543\ K$	0.140		
		$\frac{c}{24}\left(3(2c + b)J_{Ni^{2+}} - 8b(U_{Mn^{3+}} + U_{Ni^{2+}})\right)\sin\alpha = -5{,}139\ K$	0.720		
3-4	α = 95° β = 99°	$\frac{bc}{3}2J_{Ni^{2+}}(\sin\alpha + \sin\beta) = 5{,}522\ K$	0.140	-3.630	-4.599
		$\frac{c}{18}\left[\left(3cJ_{Ni^{2+}} - 4b(U_{Ni^{2+}} + U_{Mn^{4+}})\right)\sin\alpha + (3cJ_{Ni^{2+}} - 8bU_{Ni^{2+}})\sin\beta\right] = -7{,}797\ K$	0.140		
		$\frac{c}{24}\left[\left((3c + 4b)J_{Ni^{2+}} - 4b(U_{Ni^{2+}} + U_{Mn^{3+}})\right)\sin\alpha + \left((3c + b)J_{Ni^{2+}} - 4b(U_{Ni^{2+}} + U_{Mn^{3+}})\right)\sin\beta\right] = -4{,}599\ K$	0.720		
4-1	α = 92° β = 98°	$\frac{c}{18}\left(3cJ_{Ni^{2+}} - 4b(U_{Mn^{4+}} + U_{Ni^{2+}})\right)(\sin\alpha + \sin\beta) = -7{,}820\ K$	0.140	-3.644	-4.618
		$\frac{2}{3}bcJ_{Ni^{2+}}(\sin\alpha + \sin\beta) = 5{,}538\ K$	0.140		
		$\frac{c}{24}\left[\left((3c + b)J_{Ni^{2+}} - 4b(U_{Mn^{3+}} + U_{Ni^{2+}})\right)\sin\alpha + \left((3c + 4b)J_{Ni^{2+}} - 4b(U_{Mn^{4+}} + U_{Ni^{2+}})\right)\sin\beta\right] = -4{,}618\ K$	0.720		
3-4	α = 117°	$\frac{1}{9}b[3cJ_{Ni^{2+}}\sin\alpha - 4bU_{Ni^{2+}}\lvert\cos\alpha\rvert] = -1{,}432\ K$	0.140	-1.061	-1.010
		$\frac{1}{108}\left[3c\left(3cJ_{Ni^{2+}} - 4b(U_{Ni^{2+}} + U_{Mn^{4+}})\right)\sin\alpha + 2(9c^2J_{Ni^{2+}} + 8b^2J_{Mn^{4+}})\lvert\cos\alpha\rvert\right] = -0{,}948\ K$	0.140		
		$\frac{c}{48}\left((b + 3c)J_{Ni^{2+}} - b(U_{Ni^{2+}} + U_{Mn^{3+}})\right)(\sin\alpha + \lvert\cos\alpha\rvert) = -1{,}010\ K$	0.720		
3-1	α = 121°	$\frac{4}{3}b\left(cJ_{Ni}\sin\alpha - \frac{4}{3}b^2U_{Ni}\cos\alpha\right)$	1	-1.794	-1.794
4-2	α = 165°	$\frac{1}{27}(8b^2J_{Mn^{4+}} + 9c^2J_{Ni^{2+}})\lvert\cos\alpha\rvert = 3{,}293\ K$	0.140	-0.682	0.558

		$-\frac{8}{9}b^2U_{Ni^{2+}}\lvert\cos\alpha\rvert = -11{,}037\ K$	0.140		
		$\frac{1}{36}\left(9c^2J_{Ni^{2+}} + 2b^2(3J_{Mn^{3+}} - U_{Mn^{3+}} - U_{Ni^{2+}})\right)\lvert\cos\alpha\rvert = 0{,}558\ K$	0.720		

As can be seen from Table 5, the average interaction 4-4 is strengthened, when 4-3 and 4-1 are weakened.

In ludwigite structure, one can distinguish two main structural elements presented by the three leg ladders (3LL). The first 3LL is formed by ions in the positions 4-2-4 (blue octahedra in Figure 1), the second 3LL is 3-1-3 (white octahedra in Figure 1). The exchange interaction 4-3 and 4h-2a are responsible for the interaction between the 4-2-4 and 3-1-3 three-legged ladders. The magnetic structure studies of the Fe [2, 3], Co [7], Cu-Mn ludwigite showed that the magnetic structure is divided into two subsystems formed by 3LLs. In the Fe ludwigite, the magnetic moments in the subsystems are mutually orthogonal, in the Cu-Mn ludwigite, the angle between the magnetic moments of the subsystems is 60°. In the Co ludwigite, the trivalent cobalt passes into the low-spin state to reduce frustrations. For other known ludwigites, the magnetic structure has not been studied, but there is an indirect evidence that there are two magnetic subsystems. Apparently, such decomposition is the result of the crystal structure geometry. Exchange path between two 3LLs form numerous triangular groups (Figure 9a, b) and if the interaction is antiferromagnetic, it leads to a frustration in the system. A striking example is Fe ludwigite, the exchange interactions between the 3LLs are compensated, which probably leads to mutually orthogonal orientation of the magnetic moments in the subsystems [2]. It seems that in the studied ludwigite, the weakening of the exchange coupling between the subsystems increases the ordering temperature, which may be indirect evidence that the magnetic system is also divided into two subsystems. In comparison with the Ni_2MnBO_5 remanence is decreased.

When comparing these two compounds, one can see that there is no change in the 3-1-3 subsystem, since this system is formed by Ni^{2+} ions, both in one and the other compounds. All changes take place in subsystem 4-2-4.

Ions of tri- and tetravalent manganese, like bivalent nickel, occupy position 4, position 2 is occupied mainly by nickel ions. A disordered arrangement of ions in the three-legged ladders was modeled, and exchange interactions in this subsystem were considered.

The Figure 9 (a, b) shows the ions 3 and 1 neighboring triad 4-2-4, as can be seen from theFigure 10, the nickel ions in position 4h have a strong exchange interaction with its neighbors, two of which are opposite in sign to the exchange with manganese ions.

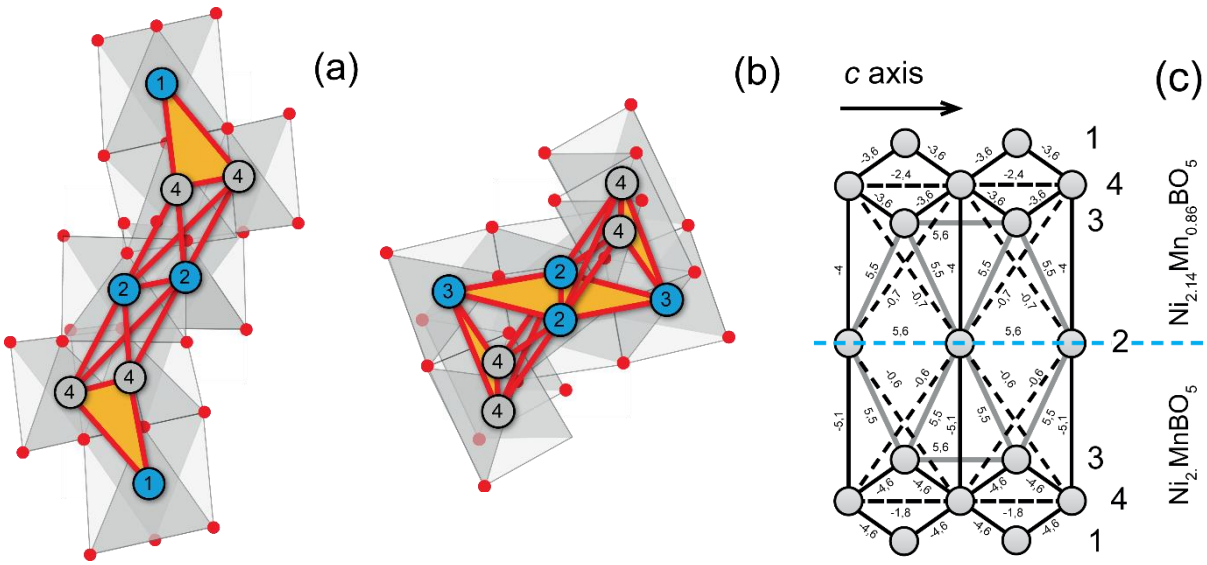

Figure 9. a, b - the triangular groups connecting the 3LL of triads 4-2-4 and 3-1-3; c - comparison of the exchanges in the triangular groups for the two compositions.

As can be seen from the Figure 10, in 3LL 4-2-4, the strong AFM interactions Ni-Ni (165°) and Ni-Mn^{4+} have appeared, however, 90° interactions Ni-Ni is FM. After averaging, 90° interactions are weakening, and 180° interaction changes its sign but remains weak. AFM interaction 4-4 enhances, however it can be not enough to double magnetic cell along *c* axis because all other exchanges – 2-2, 3-3, 1-1 – are FM and strong.

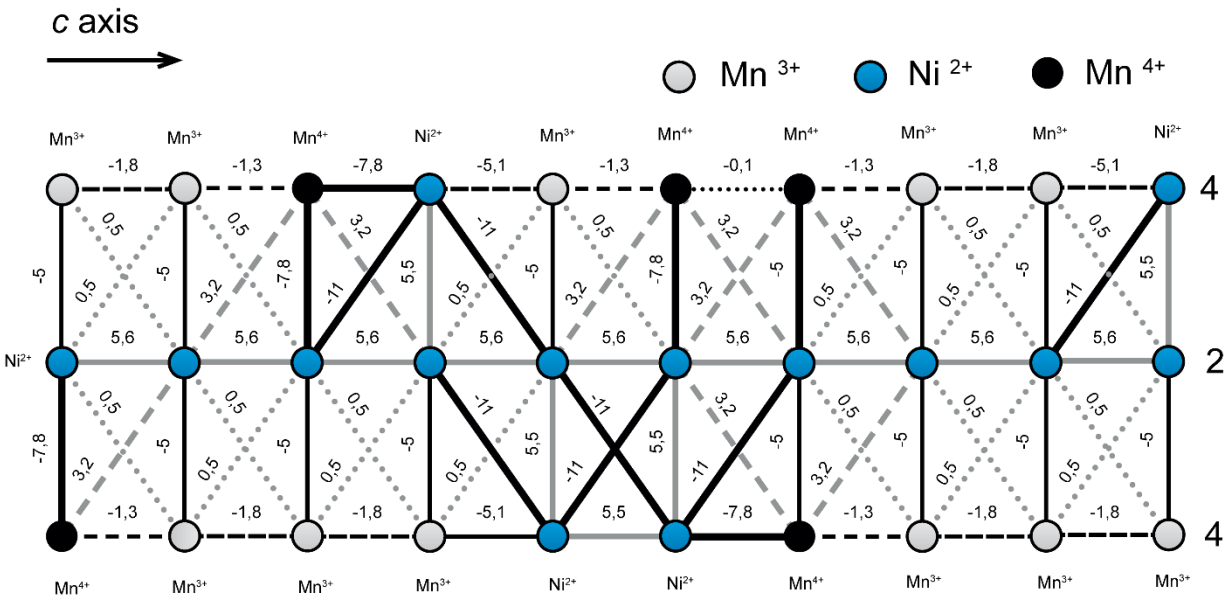

Figure 10. The 3LL of triads 4-2-4 with the designation of the exchange interactions between the ions of different types.

As we noted above, the structure geometry is formed by triangle groups of 4-1 and 4-3 bonds (Figure 9 a, b), and how one can see in the Figure 9c exchange interactions in the studied compound becomes close in magnitude that leads to the frustrations enhancement and most likely the 4-2 and 3-1 subsystems moments rotations to each other.

In the paper [11], we have assumed that the magnetic moments in the position 4 are antiferromagnetic to the moments in the position 2. The strong AFM interaction of Ni-Ni (165°) and Ni-Mn^{4+} (90°) stabilize the orientation of the ions moments.

However, the question of the magnetic moments orientation along the *c* axis remains, the position 2 imposes an FM ordering, the position 4 imposes the AFM ordering. In one and the other case, there are frustrating interactions.

3.2. Energies Estimation

Next, we analyzed the magnetic order by averaging the contributions to the exchange interaction of the various ions in 4h position. The figure shows 3LL 4-2-4 and its surrounding ions in the positions 3 and 1.

From the Figure 9c and Table 5, it is clear, that 4-4 antiferromagnetic interaction is enhanced, in addition to 180° exchange 4-2 which changes sign, although remains very weak.

Ions in the positions 1 and 3 are forming the triangular groups relative to the ion in position 4.

In the studied compound, exchanges in triangular groups are closer in magnitude and increase the frustration that likely leads to the orientation of the spins in the subsystems 3-1-3 and 4-2-4 at angles relative to each other, as in Fe_3BO_5 and Cu_2MnBO_5.

To understand what type of ordering including along the *c* axis is favorable, we estimate the energy of possible magnetically ordered structures:

$$E = -\sum_{ij} J_{ij} s_i s_j$$

The results of the calculation for both the studied compound and for the Ni_2MnBO_5 for three cases are shown in Table 6. In the first case we have assumed that all the magnetic moments are oriented collinearly, in the second case, we have assumed that the magnetic moments in the 3LLs 4-2-4 and 3-1-3 are oriented at the angle of 60°, and in the third case, the magnetic moments in sublattices are oriented orthogonally to each other. As can be seen from the Table 6, in the first and second case, the energy of ferrimagnetic structure for both compositions has the lowest value. In the first case, in the studied compound and the Ni_2MnBO_5, the energy is virtually identical. In the second case, when the magnetic moments in the subsystems 4-2 and 3-1 oriented at 60 degrees to each other, the energy of the ferrimagnetic structure in the studied compound is slightly lower than the Ni_2MnBO_5, which is consistent with experimental data, according to which the studied compound magnetic order is set at a higher temperature than in Ni_2MnBO_5. In the third case, when the magnetic moments in sub-systems 4-2 and 3-1 are oriented orthogonally, the antiferromagnetic magnetic structure has the lowest energy, which in the first and in the second case is close in energy to the ferrimagnetic. Just as in the latter case, the energy in the studied compound is slightly larger than in the Ni_2MnBO_5. Since we do not consider any other exchange interactions but superexchange, we cannot say what kind of structure is realized, but the growth of the energy in this compound, with the approach of the orientation of magnetic moment in subsystems to orthogonal can be seen in the calculation. As we have noted, in Cu_2MnBO_5 and Fe_3BO_5, magnetic moments in the subsystems are deployed in relation to each other, frustrations are also presented in triangular groups 3-4-3 and 1-4-1 in the studied compound, and they are amplified in comparison with the Ni_2MnBO_5, that may lead to reverse of the magnetic moments in the sublattices.

Table 6. Energies of the different magnetic structures for two compounds.

Positions				**Type**	**0°**			**60°**		**90°**	
1	2	3	4		E(st.sam.), K	E(Ni_2MnBO_5), K	μ/mol	E(st.sam.)/u.c., K	E(Ni_2MnBO_5), K	E(st.sam.)/u.c., K	E(Ni_2MnBO_5), K
↓↓	↓↓	↓↓↓↓	↑↑↑↑	FIM	**-252**	**-253**	-0.42	**-155**	**-149**	-58	-45
↓↑	↑↓	↑↑↓↓	↓↓↑↑	AFM	-228	-235	0	-150	-147	**-72**	**-59**
↓↑	↓↓	↓↓↓↓	↑↑↑↑	FIM	-194	-186	0.58	-129	-119	-65	-52
↓↑	↑↓	↓↑↓↓	↑↓↑↑	AFM	-168	-170	0.79	-107	-104	-47	-37
↓↑	↑↓	↓↑↓↓	↓↓↑↑	FIM	-179	-180	-1	-124	-118	-69	-56
↓↑	↓↓	↓↑↓↓	↑↓↑↑	FIM	-168	-170	-0.21	-107	-104	-47	-37
↓↓	↓↑	↓↓↓↓	↑↑↑↑	FIM	-165	-172	0.58	-90	-90	-15	-8
↓↑	↓↓	↓↓↓↓	↓↑↑↑	FIM	-163	-160	-1.21	-103	-97	-44	-34
↓↓	↓↓	↓↓↓↑	↑↑↑↓	FIM	-160	-163	-1.21	-100	-97	-40	-30
↓↓	↓↓	↓↓↓↓	↑↑↓↑	FIM	-156	-153	-2.21	-96	-90	-37	-27

In Table 6, we only have shown the several types magnetically ordered states calculation which is most favorable in energy, though the calculation was performed for all possible ordering variants in the unit cell and the cell doubled along the shortest axis. The doubling of the magnetic cell is not profitable, despite the fact that the antiferromagnetic exchange between the ions in the position along the *c* axis increases.

It should be noted that several types of ordering are close enough in energy for all cases of the sublattices magnetic moments orientation relative to each other, the temperature dependence of the magnetization has a bend near the 70 K. The remanence derived from the hysteresis loop is sufficiently small -0.021 μ_B. In Table 6, we have given the saturation magnetization for the different type of ordering at the collinear orientation, as can be seen from the table, the experimental value more than an order of magnitude less than the calculated values, apparently, the studied compound is more beveled antiferromagnet than ferrimagnet. As can be seen from Table 6, the residual magnetization with the collinear ordering of the magnetic moments is at least an order of magnitude larger than the experimental values. Since we consider only superexchange interaction and do not consider the direct exchange and super-superexchange interactions through boron ions, the energy of the ferromagnetic and antiferromagnetic states are very close. It is likely that, in reality, the antiferromagnetic structure is realized.

Conclusion

In the course of the study, we managed to obtain a compound with a ludwigite structure, in which manganese enters in two different valence states: tri- and tetravalent states. The composition of the studied compound was refined by a jump on the absorption of manganese and nickel ions K-edge, the chemical formula of the compound obtained: $Ni_{2.14}Mn_{0.86}BO_5$. Despite the fact that in the studied compound due to the presence of manganese in the different valence states, the degree of disorder is higher than in the Ni_2MnBO_5, the magnetic order transition temperature in the studied compound is 15 K higher. Held within the empirical model of Anderson-Zawadsky exchange interactions analysis showed that frustrations are amplified in triangular groups 3-4-3 and 1-4-1, which can lead to the non-collinear orientation of magnetic moments in the sublattices 4-2-4 and 3-1-3. In the case where magnetic moments in the sublattices 4-2-4 and 3-1-3 are oriented at an angle of 60° and 90°, the most beneficial energetically magnetic structure in the studied compound is lower than in the Ni_2MnBO_5 (Figure 11), which is consistent with experimental data, according to which magnetic ordering is observed in the studied compound at a higher temperature. Energies of several magnetically ordered states are close enough.

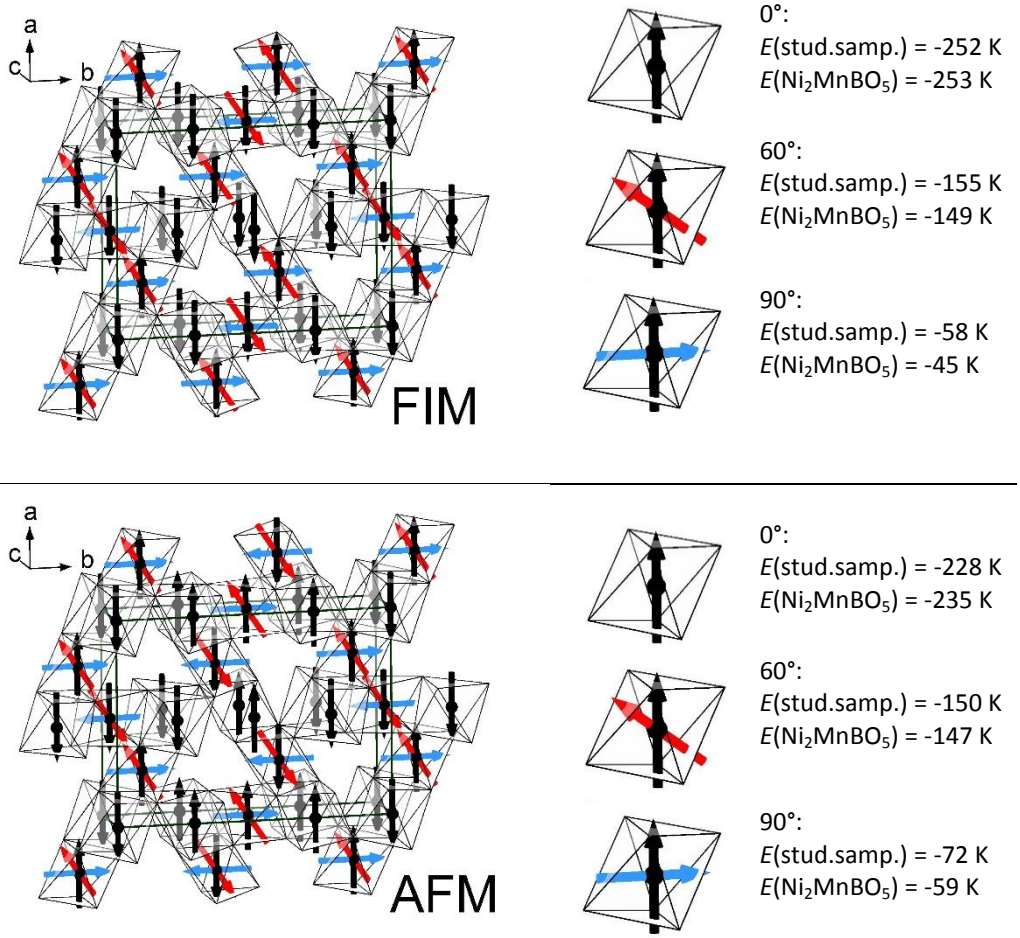

Figure 11. The most energetically preferable magnetic structures with energy values for both compositions. Note that only one color arrow in the octahedron is applicable for the selected configuration.

Acknowledgement

Russian Foundation for Basic Research (RFBR) and Government of Krasnoyarsk Territory supported this study according to the research project No. 17-42-240338.

References

[1] S. Sofronova and I. Nazarenko, "Ludwigites: From natural mineral to modern solid solutions," *Crystal Research and Technology,* p. Early View (Online Version of Record published before inclusion in an issue), 2017.

[2] J. P. Attfield, J. F. Clarke and D. A. Perkins, "Magnetic and crystal structures of iron borates," *Physica B: Condensed Matter,* Vols. 180-181, pp. 581-584, 2 June 1992.

[3] P. Bordet and E. Suard, "Magnetic structure and charge ordering in Fe3BO5: A single-crystal x-ray and neutron powder diffraction study," *Physical Review B,* vol. 79, p. 144408, 9 April 2009.

[4] D. C. Freitas, R. B. Guimarães, D. R. Sanchez, J. C. Fernandes, M. A. Continentino, J. Ellena, A. Kitada, H. Kageyama, A. Matsuo, K. Kindo, G. G. Eslava and L. Ghivelder, "Structural and magnetic properties of the oxyborate Co5Ti(O2BO3)2," *Physical Review B,* vol. 81, p. 024432 , 29 January 2010.

[5] S. N. Sofronova, L. N. Bezmaternykh, E. V. Eremin, I. I. Nazarenko, N. V. Volkov, A. V. Kartashev and E. M. Moshkina, "The superexchange interactions and magnetic ordering in low-dimentional ludwigite Ni5GeB2O10," *Journal of Magnetism and Magnetic Materials,* vol. 401, p. 217–222, 1 March 2016.

[6] C. P. C. Medrano, D. C. Freitas, D. R. Sanchez, C. B. Pinheiro, G. G. Eslava, L. Ghivelder and M. A. Continentino, "Nonmagnetic ions enhance magnetic order in the ludwigite Co5Sn(O2BO3)2," *Physical Review B,* vol. 91, p. 054402 , 4 February 2015.

[7] D. C. Freitas, C. P. C. Medrano, D. R. Sanchez, R. M. Nuñez, J. A. Rodríguez-Velamazán and M. A. Continentino, "Magnetism and charge order in the ladder compound Co3O2BO3," *Physical Review B,* vol. 94, p. 174409 , 4 November 2016.

[8] L. N. Bezmaternykh, E. M. Kolesnikova, E. V. Eremin, S. N. Sofronova, N. V. Volkov and M. S. Molokeev, "Magnetization pole reversal of ferrimagnetic ludwigites Mn3-xNixBO5," *Journal of Magnetism and Magnetic Materials,* p. 55–59, September 2014.

[9] Bruker AXS TOPAS V4: General profile and structure analysis software for powder diffraction data. User's Manual, Karlsruhe: Bruker AXS, 2008.

[10] K. Bluhm and H. Müller-Buschbaum, "About the Stabilization of the Oxidation State MIV in the Ni5MB2O10-Type (M=V4+, Mn4+)," *Zeitschrift für anorganische und allgemeine Chemie,* vol. 579, no. 1, pp. 111-115, 1989.

[11] E. Moshkina, S. Sofronova, A. Veligzhanin, M. Molokeev, I. Nazarenko, E. Eremin and L. Bezmaternykh, "Magnetism and structure of Ni2MnBO5 ludwigite," *Journal of Magnetism and Magnetic Materials,* vol. 402, pp. 69-75, 15 March 2016.

[12] L. Bezmaternykh, E. Moshkina, E. Eremin, M. Molokeev, N. Volkov and Y. Seryotkin, "Spin-Lattice Coupling and Peculiarities of Magnetic Behavior of Ferrimagnetic Ludwigites Mn0.52+M1.52+Mn3+BO5(M=Cu, Ni)," *Solid State Phenomena,* Vols. 233-234, pp. 133-136, 2015.

[13] A. A. Chernyshov, A. A. Veligzhanin and Y. V. Zubavichus, "Structural Materials Science end-station at the Kurchatov Synchrotron Radiation Source: Recent instrumentation upgrades and experimental results," *Nuclear Instruments and Methods in Physics Research Section A: Accelerators, Spectrometers, Detectors and Associated Equipment,* vol. 603, no. 1-2, pp. 95-98, 11 May 2009.

[14] S. Sofronova, E. Moshkina, I. Nazarenko, Y. Seryotkin, S. Nepijko, V. Ksenofontov, K. Medjanik, A. Veligzhanin and L. Bezmaternykh, "Crystal growth, structure, magnetic properties and theoretical exchange interaction calculations of Cu2MnBO5," *Journal of Magnetism and Magnetic Materials,* vol. 420, pp. 309-316, 15 December 2016.

[15] M. Newville, "IFEFFIT : interactive XAFS analysis and FEFF fitting," *Journal of Synchrotron Radiation,* vol. 8, pp. 322-324, 2001.

[16] B. Ravel and M. Newville, "ATHENA, ARTEMIS, HEPHAESTUS: data analysis for X-ray absorption spectroscopy using IFEFFIT," *Journal of Synchrotron Radiation,* vol. 12, pp. 537-541, 2005.

[17] G. A. Bain and J. F. Berry, "Diamagnetic Corrections and Pascal's Constants," *Journal of Chemical Education,* vol. 85, no. 4, p. 532, 2008.

[18] K. Sugawara, N. Arai, A. Kouzuki, K. Hotta, H. Hirose and C. W. Chu, "ESR Studies on GMR Related Materials IV: ESR of Mn in La0.7Ca0.3MnO3," *Modern Physics Letters B,* vol. 15, p. 331, 2001.

[19] Y. N. Khakimullin, V. S. Minkin, T. R. Deberdeev and G. E. Zaikov, Polysulfide Oligomer Sealants: Synthesis, Properties and Applications, Apple Academic Press, 2015, p. 95.

[20] E. A. Zverevaa, V. B. Nalbandyan, M. A. Evstigneeva, K. Hyun-Joo, M.-H. Whangbo, A. V. Ushakov, B. S. Medvedev, L. I. Medvedeva, N. A. Gridina, G. E. Yalovega, A. V. Churikov, A. N. Vasiliev and B. Büchner, "Magnetic and electrode properties, structure and phase relations of the layered triangular-lattice tellurate Li4NiTeO6," *Journal of Solid State Chemistry,* vol. 225, pp. 89-96, May 2015.

[21] P. W. Anderson, "New Approach to the Theory of Superexchange Interactions," *Physical Review,* vol. 115, no. 1, p. 2, 1 July 1959.

[22] O. A. Bayukov and A. F. Savitskii, "The Prognostication Possibility of Some Magnetic Properties for Dielectrics on the Basis of Covalency Parameters of Ligand-Cation Bonds," *Physica Status Solidi b,* vol. 155, no. 1, p. 249–255 , 1 September 1989.